Nanostructures

Deutsche Ausgabe: DOI: 10.1002/ange.201606469
Internationale Ausgabe: DOI: 10.1002/anie.201606469

Biomimetic Nanofluidic Diode Composed of Dual Amphoteric Channels Maintains Rectification Direction over a Wide pH Range

Xin Sui[+], Zhen Zhang[+], Zhenyu Zhang[+], Zhiwei Wang[+], Chao Li, Hao Yuan, Longcheng Gao, Liping Wen,* Xia Fan,* Lijun Yang, Xinru Zhang, and Lei Jiang*

Abstract: *pH-gated ion channels in cell membranes play important roles in the cell's physiological activities. Many artificial nanochannels have been fabricated to mimic the natural phenomenon of pH-gated ion transport. However, these nanochannels show pH sensitivity only within certain pH ranges. Wide-range pH sensitivity has not yet been achieved. Herein, for the first time, we provide a versatile strategy to increase the pH-sensitive range by using dual amphoteric nanochannels. In particular, amphoteric polymeric nanochannels with carboxyl groups derived from a block copolymer (BCP) precursor and nanochannels with hydroxyl groups made from anodic alumina oxide (AAO) were used. Due to a synergistic effect, the hybrid nanochannels exhibit nanofluidic diode properties with single rectification direction over a wide pH range. The novel strategy presented here is a scalable, low-cost, and robust alternative for the construction of large-area membranes for nanofluidic applications, such as the separation of biomolecules.*

Ion transport through the biological nanochannels of cell membranes is important for maintaining an organism's physiological activities.[1] For example, the influenza M_2 protein, a well-known pH-gated ion channel, plays a critical role in virus uncoating.[2] The pH-sensitive ion transport depends mainly on the amphoteric residues along the channel. By tuning the ionization states of the functional groups at different pH values, the microenvironment of the channels is changed. As a result, the charge distribution affects ion transport, and consequently, also affects the processes that cells perform to maintain essential life activities, such as diffusion, osmosis, and phagocytosis[3] Many artificial nanochannels have been designed to mimic the phenomena in the living systems. For example, an asymmetric chemical modification of an hourglass-shaped nanochannel has pH-gating ion transport properties.[4] Conical single nanochannels grafted with zwitterionic polymers or proteins exhibit pH-tunable rectifying characteristics.[5] Amphoteric conical nanopores functionalized with lysine and histidine groups give remarkable rectification characteristics at different pH values.[6] Artificial ion-transport nanochannels that display ionic selectivity, ionic rectification, and ionic gating in response to pH are of general interest because of the potential applications in biosensing,[5,7] molecular filtration,[8] and energy harvesting[9]. However, these pH sensitive systems show narrow pH windows, that is, they are only activated at certain pH values, or reverse their rectification directions when the local pH values change from acidic to basic, which limits their practical applications. It is desirable to construct a biomimetic nanofluidic diode with a single rectification direction over a wide pH range, preferably by using a simple, versatile, engineered methodology.

Nanochannels have been produced using various fabrication techniques, including ion track etching,[10] electrochemical etching,[11] laser technology,[12] and high energy beam etching.[13] These methods, typically followed by complicated structural/chemical modification, only realize monotonic functionality. In this work, we present an optimized, indirect, and scalable strategy. With the combination of dual amphoteric nanochannels, a nanofluidic diode with a single rectification direction over a wide pH range is achieved. Two kinds of nanochannels with differential diameters and amphoteric characteristics were prepared independently. Nanochannels with carboxyl groups were derived from block copolymer (BCP) precursors. BCPs are one of the most important materials for the creation of nanostructures. BCPs self-assemble into well-defined nanostructures with suitable volume fractions and Flory–Huggins interaction parameters.[14] Nanoporous structures are formed by removing one block from the BCP, and functional terminal groups are

[*] Dr. X. Sui,[+] Z. W. Wang,[+] C. Li, Prof. Dr. L. C. Gao, Prof. Dr. X. Fan, Prof. Dr. L. Jiang
Laboratory of Bio-Inspired Smart Interfacial Science and Technology of Ministry of Education, Key Laboratory of Beijing Energy, School of Chemistry and Environment, Beihang University
Beijing 100191 (P.R. China)
E-mail: lcgao@buaa.edu.cn
fanxia@buaa.edu.cn

Dr. Z. Zhang,[+] Prof. Dr. L. P. Wen, Prof. Dr. L. Jiang
Key Laboratory of Bio-inspired Materials and Interfacial Science, Technical Institute of Physics and Chemistry
Chinese Academy of Sciences
Beijing 100190 (P.R. China)
E-mail: wen@mail.ipc.ac.cn

Dr. Z. Y. Zhang[+]
Beijing National Laboratory for Molecular Sciences, Key Laboratory of Polymer Chemistry and Physics of Ministry of Education, College of Chemistry and Molecular Engineering, Peking University
Beijing, 100871 (P.R. China)

Dr. H. Yuan, Prof. Dr. X. R. Zhang
School of Mechanical Engineering
University of Science and Technology Beijing
Beijing, 100083 (P.R. China)

Prof. Dr. L. J. Yang
School of Astronautics, Beihang University
Beijing, 100191 (P.R. China)

[+] These authors contributed equally to this work.

Supporting information for this article can be found under: http://dx.doi.org/10.1002/anie.201606469.

retained on the inner surface of the nanopores.[15] In particular, carboxyl groups are generated by default upon UV exposure when a UV sensitive *o*-nitrobenzyl ester (ONB) is used as the junction of the BCPs.[15d,16] The pore size can be tuned from 5 to 100 nm. The other nanochannels were obtained from anodic alumina oxide (AAO) membranes. AAO membranes possess uniform and nearly parallel pores with diameters that can be varied from <10 to 200 nm by changing the anodization parameters.[17] Additionally, the surfaces of AAO nanochannels have pH-dependent surface charges as a result of the amphoteric OH groups. By transferring the polymeric membranes onto the AAO membranes, asymmetric organic–inorganic hybrid nanochannels can be formed. The hybrid nanochannels are composed of polymeric and AAO pores containing carboxyl and hydroxyl groups, respectively (Figure 1 A). Because of the protonation state of the nanochannels under different pH conditions, ion transport through the nanochannels can be tuned and exhibits unique nanofluidic diode properties.

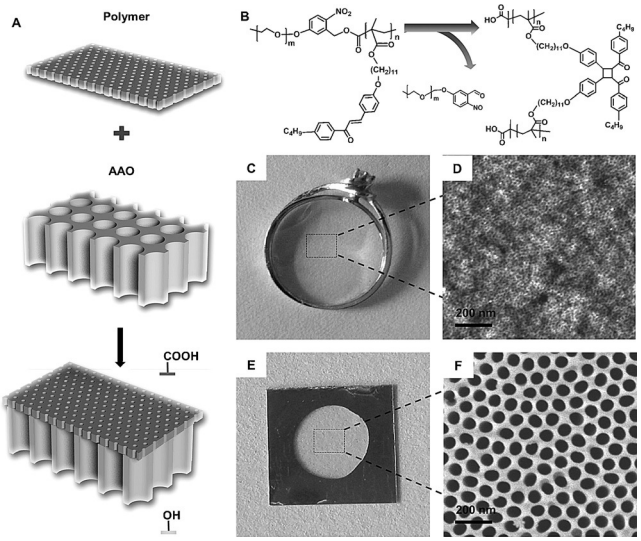

Figure 1. A) The fabrication of bioinspired nanofluidic diode with dual amphoteric nanochannels. The polymeric nanochannel is derived from a BCP precursor, while the other is an AAO membrane. B) The molecular design of the BCP PEO-*hν*-PChal containing a UV-degradable linker between the blocks and UV-crosslinkable chalcone groups in one of the blocks. After self-assembly and UV irradiation, nanochannels bearing carboxyl groups are prepared. C) The resultant membrane is free-standing. D) AFM height image of membrane surface shows that well-defined nanopores have formed. E) AAO membranes are made and nanochannels across the membrane can be seen in F) the top-view SEM image.

First, the UV sensitive BCP precursor was designed and prepared (see Figure 1 B and the Supporting Information, Figure S1). The BCP contains the ONB group as the junction for the building blocks. Additionally, the blocks contain poly(ethylene oxide) (PEO), which is soluble in most solvents, and poly(methacrylate) with chalcone (PChal) as the UV-crosslinkable unit.[18] This BCP, which is referred to as PEO-*hν*-PChal, contains cleavable junctions and crosslinkable units in a single chain. During UV exposure, chain cleavage and crosslinking occur simultaneously.

The PEO macroinitiator was synthesized by click chemistry, which was confirmed by ^{1}H NMR spectroscopy (Supporting Information, Figure S2). After that, BCP was synthesized by atom-transfer radical polymerization (ATRP) from the PEO macroinitiator. Compared with the PEO macroinitiator, a remarkable unimodal shift to higher molecular weight was observed by gel-permeation chromatography (GPC) (Supporting Information, Figure S3). The BCP has a molecular weight of 27300 g mol^{-1} and a polydispersity index of 1.25. The ^{1}H NMR spectrum of the BCP shows that the characteristic peaks of the chalcone groups are located in the range of 6.8 to 7.9. From the integrated peaks, the weight fraction of PEO in the BCP is calculated to be 17.6%.

The BCP then underwent UV-cleavage and crosslinking. As shown in the Supporting Information, Figure S4 A, the intensity of the absorption band near 300 nm, which is associated with the nitro-aromatic linker, clearly decreases during UV irradiation (365 nm), demonstrating the successful cleavage of the ONB group.[15f] Under the same UV irradiation conditions, photodimerization of the chalcone mesogens occurs simultaneously with the linker cleavage, as confirmed by the decrease in intensity of the peak near 340 nm.[19]

The successful removal of PEO and crosslinking of PChal through UV treatment are further demonstrated by IR spectroscopy (Supporting Information, Figure S4 B). In the original BCP thin film, the peaks at 1146 and 982 cm^{-1} are assigned to the C–*O*–C stretching and CH_2 rocking modes in PEO, respectively.[15h,20] Both of these peaks disappear after removal of the PEO. The photo-crosslinking of the chalcone mesogens is also verified by the disappearance of the peaks at 1660 and 1587 cm^{-1}, which correspond to C=O and C=C groups, respectively, after UV irradiation.[21] Carboxyl groups are generated after cleavage of the ONB group, as evidenced by the appearance of a broad peak at 3300 cm^{-1}.

The BCP precursor used self-assembles into hexagonally packed cylindrical nanostructures. In the Supporting Information, Figure S5, we see separated nanodots dispersed into hexagonal patterns. The dots are the PEO cylinders, which are selectively stained by RuO_4. The PEO cylinders are oriented perpendicularly over the entire surface. The perpendicularly oriented cylindrical structure is important for the applications. The center-to-center distance between the PEO cylinders is approximately 20 nm, and the diameter of the PEO cylinders is approximately 5 nm.

Self-standing nanoporous membranes are desirable for the fabrication of bilayer organic–inorganic hybrid nanochannels. After UV treatment of the BCP self-assembled precursor, extraction of the PEO homopolymer, and dissolution of the sacrificial layer (Supporting Information, Figure S6), a free-standing nanoporous membrane was successfully removed from the substrate and attached to a ring for support (Figure 1 C). The membrane is stable in the laboratory environment and remains unchanged for several weeks. AFM was used to observe the structure of the nanopores. Figure 1 D shows the AFM topography image of the membrane after UV treatment. From the image, hexagonally-

packed nanopores were observed, indicating that the nanoporous film retains long-range order throughout the UV treatment process.

As mentioned above, in situ carboxyl groups remain on the inner surface of the nanochannels after UV treatment. The presence of carboxyl groups on the nanostructures is reflected by the zeta potential measurements of the membrane as a function of pH (Supporting Information, Figure S4C). The zeta potentials are negative at high pH values. As the pH decreases, the zeta potential increases to nearly zero and even becomes slightly positive. The dependence of the zeta potential on pH is characteristic of a weakly acidic surface.[22]

When the organic nanochannels were prepared, the inorganic nanochannels were fabricated by using an anodization process. SEM measurements of the AAO membrane reveal nanochannels with diameters of circa 80 nm (Figure 1E,F). The rigid AAO membrane has good mechanical properties and works as a support for the PChal membrane. As shown in Figure 1A, by transferring the polymeric membrane onto the AAO membrane, asymmetric hybrid nanochannels are formed (Supporting Information, Figure S8). Both membranes are of different thickness. The PChal membrane's thickness is two orders of magnitude smaller than that of the AAO membrane, to ensure that the ordered cylindrical structures are perpendicular to the membrane surface. Aside from the differences in the nanochannels' diameters, the functional groups on the surface of the nanochannels are also different between the two membranes, which will be discussed later. The nanochannel surface groups can be used as the modification sites to extend the application scope. For example, diamine molecules can easily react with the carboxyl groups to generate a positively charged surface. pH-responsive hybrid nanotubes have been fabricated by an AAO-template-assisted assembly method, and have intriguing applications in sensing and microfluidic systems.[23] Our hybrid membrane has additional advantages, such as the stability that results from the crosslinked structure.

The transport of ions through the membrane was measured using a transmembrane electrical potential that was scanned from −2 V to +2 V (see the Supporting Information, Figure S9). For an AAO nanoporous membrane, the current–potential (*I–V*) curves are all linear and thus follow Ohm's law in the pH range from 3 to 11. The nanochannels do not demonstrate ion-gating characteristics (see Figure 2A). After loading the PChal membrane onto the AAO membrane, the rectification ratio reached 9.7 at a pH of 3 as shown in Figure 2B,C. In an alkaline solution (pH 11), the ionic current rectification ratio of the hybrid membrane is 11.0. At a pH of 7, the rectification ratio of the hybrid membrane is 4.9. Notably, the magnitudes of the currents at positive potentials (ON state) are higher than those at negative potentials (OFF state) for all the pH conditions. For the first time, we obtained artificial nanochannels with the same ion rectification direction over a wide pH range from acidic to basic conditions.

The unique ion transport properties of the hybrid nanochannels are attributed to the synergistic effect of the nanoporous AAO and polymeric membrane with different pore sizes and functional groups. AAO has amphoteric

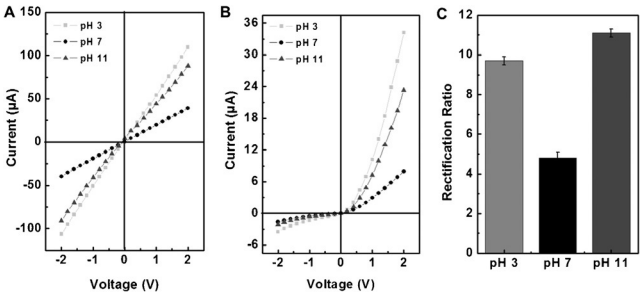

Figure 2. Composite membrane *I–V* curves for A) AAO nanochannels and B) hybrid nanochannels measured in KCl solution at various pH values. C) The rectification ratio of hybrid nanochannels.

properties. The isoelectric point (IEP) of AAO is approximately 8.7 (Supporting Information, Figure S7). On the surface, AAO reacts with H^+ or OH^- in acidic or basic solutions to form $Al{-}OH_2^+$ or $Al{-}O^-$ groups, respectively. Carboxyl groups are present on the PChal nanochannel's surface. Thus, the surface charges on both the AAO and PChal nanochannels can be modulated by adjusting the pH of the electrolyte.

In particular, at a pH of 11, both the AAO and PChal nanochannels have negatively charged surfaces (Figure 3A-I). The experimentally observed diode-like behavior could be attributed to the broken symmetry of the electrochemical potential inside the nanochannel, similar to the case of a negatively charged conical nanochannel (Figure 3A-II,III). The cations will flow preferentially from the PChal membrane to the AAO nanochannel, resulting in a much higher positive ionic current. When the heterogeneous nanochannel is placed in the electrolyte solution with a pH of 3, the AAO nanochannels are positively charged and the PChal nanochannels are uncharged (Figure 3C-I). Therefore, the surface charge distribution is asymmetric along the length of the hybrid nanochannel. The corresponding *I–V* curve has diode-like characteristics similar to that measured at the pH of 11. In this condition, the system functions as a unipolar nanofluidic diode that is composed of a junction between a neutral PChal channel and a positively charged AAO channel, in which the AAO side performs a dominant role (Figure 3C-II,III). The positive bias will drive the anions attracted in the AAO side towards the interfacial junction, forming an ion-enrichment region. On the contrary, a reversed bias will contribute to the formation of an ion-depletion region and a rectified ionic current can be observed.

At a pH of 7, which is between the IEP of AAO and the pKa of PChal, the AAO and PChal nanochannels are slightly positively and negatively charged, respectively. The surface charge distribution of the heterogeneous nanochannel is Janus-like (Figure 3B-I), functioning as a bipolar nanofluidic diode (Figure 3B-II,III). Under a forward bias, cations (K^+) are preferentially attracted to the PChal side and migrate to the interfacial region. Meanwhile, anions (Cl^-) are preferentially attracted from the AAO side and migrate to the same interfacial region. The convection of cations and anions will form an ion-enrichment region. Under a reverse bias, ion transport proceeds in the opposite direction, causing an ion-depletion region. The rectification ratio is approximately 4.9,

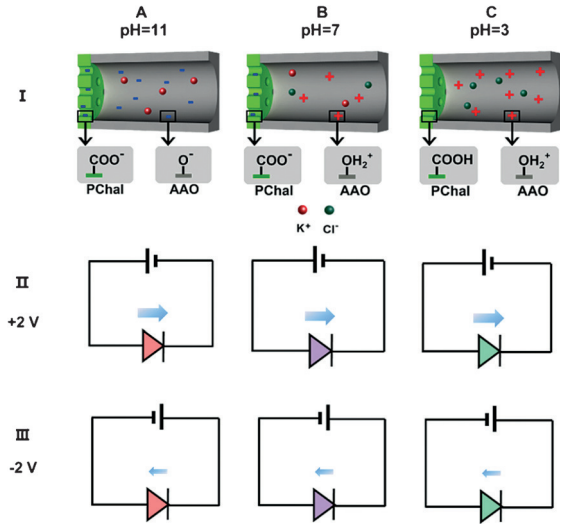

Figure 3. Ion migration in the hybrid nanochannels at different pH values. A) At a pH of 11, both the PChal and AAO nanochannels surfaces are negatively charged (I). Under a forward bias (+2 V), K^+ ions are preferentially transported from the PChal side to the AAO side of the membrane, so that the nanofluidic diode is open under forward bias (II) and closed under reverse bias (III). B) At a pH of 7, the PChal and AAO nanochannels are weakly negatively and positively charged, respectively (I). The current displays weak ion rectifying properties under these conditions (II, III). C) At a pH of 3, the PChal and AAO nanochannels are uncharged and positively charged, respectively (I). Under a forward bias, Cl^- ions are preferentially transported from the AAO side to the PChal side, so that the nanofluidic diode is open under forward bias (II) and closed under reverse bias (III).

which shows weak ion rectifying properties. In principle, a biased bipolar nanochannel can accumulate or deplete ions more efficiently than the unipolar diode. In our case, the largely decreased ionic rectification could be ascribed to the relatively low surface charge density of the heterogeneous nanochannel at pH 7.

The ionic rectification properties depend strongly on the asymmetric properties of the system such as geometry, charge distribution, and chemical composition, which can be qualitatively supported by a numerical simulation based on Poisson–Nernst–Planck (PNP) equations. The Nernst–Planck equation that describes the transport properties of charged nanochannels is shown below, where j_i, D_i, c_i, z_i, and φ are the ionic flux, diffusion coefficient, ion concentration, and valence number for each species i and the electrical potential, respectively:

$$j_i = D_i\left(\nabla c_i + \frac{z_i F c_i}{RT}\nabla\varphi\right) \quad (1)$$

The electrical potential inside the nanochannel can be related with the ionic concentration by the Poisson equation:

$$\nabla^2\varphi = -\frac{F}{\varepsilon}\sum z_i c_i \quad (2)$$

Simplified by assuming steady-state conditions, the flux should satisfy the time-independent continuity equation:

$$\nabla j_i = 0 \quad (3)$$

As previously described, the ionic rectification at different pH values derives from the ionic accumulation and depletion under different voltage bias. By applying suitable boundary conditions, the coupled equations can be solved to generate the ionic concentration distribution inside the hybrid nanochannel, from which we can qualitatively simulate the ionic rectification. For simplicity, the model was assumed to be a 2000 nm long channel (Figure S10) composed of 800 nm long BCP nanochannels and a 1200 nm long AAO nanochannel.

Both the AAO and PChal nanochannels are negatively charged at the pH value of 11 (Figure 4 A-I). The ionic

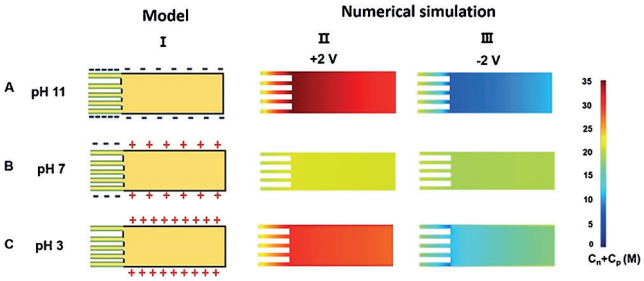

Figure 4. Numerical simulations of the ion concentration profiles at +2 and −2 V bias at different pH values.

concentration profiles of the nanochannel show great differences upon switching the external bias (Figure 4 A-II,III). The ionic concentration obtained at +2 V is much larger than that obtained at −2 V, which is ascribed to the preferential flow of cations induced by the broken symmetry of the electrical field. When we transfer the nanochannel into an acidic solution (pH 3.0), the heterogeneous nanochannel exhibits a unipolar charge distribution (Figure 4 C-I). The difference in the concentration profile becomes weakened, implying a decreased ionic rectification, which is consistent with the experimental results (Figure 4 C-II,III). If the hybrid nanochannel was placed in a solution with pH 7, the ionic rectification decreases largely, which can be seen from the concentration profile (Figure 4 B-II,III). At the pH of 7, the surface charge distribution of the system is Janus-like (Figure 4 B-I). Because of the weak charge density, the ability to accumulate or deplete ions under an external bias largely weakens, resulting in a very low rectification effect. Notably, the diameter of the nanochannels influences the rectification effect, according to the simulation shown in the Supporting Information, Figure S11. These results help us design high-performance nanofluidic diode devices.

In conclusion, a facile strategy has been developed to fabricate organic–inorganic hybrid nanochannels, which exhibit the characteristics of a biomimetic nanofluidic diode. In a wide pH range from acidic to basic, the nanodevices exhibit the same rectification direction. The different pH sensitivity of surface groups (COOH or Al–OH) corresponds to the unique phenomena. The method developed in this work is a scalable, low-cost, and robust alternative for the

construction of large area membranes for nanofluidic applications. This strategy enables new nanofluidic devices, offering potential applications in ion-exchange membranes for the separation of biomolecules.

Acknowledgements

The authors thank Dr Leung Nelson Lik Ching at the Hong Kong University of Science and Technology for helpful comments. The work was supported by National Natural Science Foundation (21434003, 91427303, 51673206, 21204002).

Keywords: amphoteric nanochannels · block copolymers · ion transport · nanofluidic diodes · ph-gating

How to cite: *Angew. Chem. Int. Ed.* **2016**, *55*, 13056–13060
Angew. Chem. **2016**, *128*, 13250–13254

[1] a) J. Hu, C. Zhong, C. Ding, Q. Chi, A. Walz, P. Mombaerts, H. Matsunami, M. Luo, *Science* **2007**, *317*, 953–957; b) G. L. Nicolson, R. Yanagimachi, *Science* **1972**, *177*, 276–279; c) T. E. Decoursey, *Physiol. Rev.* **2003**, *83*, 475–579.

[2] L. H. Pinto, L. J. Holsinger, R. A. Lamb, *Cell* **1992**, *69*, 517–528.

[3] S. Cowan, T. Schirmer, G. Rummel, M. Steiert, R. Ghosh, R. Pauptit, J. Jansonius, J. Rosenbusch, *Nature* **1992**, *358*, 727–733.

[4] X. Hou, Y. Liu, H. Dong, F. Yang, L. Li, L. Jiang, *Adv. Mater.* **2010**, *22*, 2440–2443.

[5] I. Vlassiouk, T. R. Kozel, Z. S. Siwy, *J. Am. Chem. Soc.* **2009**, *131*, 8211–8220.

[6] M. Ali, P. Ramirez, S. Mafé, R. Neumann, W. Ensinger, *ACS Nano* **2009**, *3*, 603–608.

[7] a) A. de la Escosura-Muñiz, A. Merkoçi, *ACS Nano* **2012**, *6*, 7556–7583; b) L. Lin, Y. Liu, J. Yan, X. Wang, J. Li, *Anal. Chem.* **2013**, *85*, 334–340; c) M. Ali, B. Yameen, R. Neumann, W. Ensinger, W. Knoll, O. Azzaroni, *J. Am. Chem. Soc.* **2008**, *130*, 16351–16357; d) Z. Siwy, L. Trofin, P. Kohli, L. A. Baker, C. Trautmann, C. R. Martin, *J. Am. Chem. Soc.* **2005**, *127*, 5000–5001.

[8] I. Vlassiouk, P. Y. Apel, S. N. Dmitriev, K. Healy, Z. S. Siwy, *Proc. Natl. Acad. Sci. USA* **2009**, *106*, 21039–21044.

[9] Z. Zhang, X.-Y. Kong, K. Xiao, Q. Liu, G. Xie, P. Li, J. Ma, Y. Tian, L. Wen, L. Jiang, *J. Am. Chem. Soc.* **2015**, *137*, 14765–14772.

[10] a) Y. Xu, X. Sui, S. Guan, J. Zhai, L. Gao, *Adv. Mater.* **2015**, *27*, 1851–1855; b) X. Hou, F. Yang, L. Li, Y. Song, L. Jiang, D. Zhu, *J. Am. Chem. Soc.* **2010**, *132*, 11736–11742.

[11] a) S. E. Létant, T. W. van Buuren, L. J. Terminello, *Nano Lett.* **2004**, *4*, 1705–1707; b) B. Zhang, Y. Zhang, H. S. White, *Anal. Chem.* **2004**, *76*, 6229–6238.

[12] S. Wu, S. R. Park, X. S. Ling, *Nano Lett.* **2006**, *6*, 2571–2576.

[13] a) C. Dekker, *Nat. Nanotechnol.* **2007**, *2*, 209–215; b) A. Mara, Z. Siwy, C. Trautmann, J. Wan, F. Kamme, *Nano Lett.* **2004**, *4*, 497–501; c) P. Y. Apel, Y. E. Korchev, Z. Siwy, R. Spohr, M. Yoshida, *Nucl. Instrum. Methods Phys. Res. Sect. B* **2001**, *184*, 337–346; d) A. Storm, J. Chen, X. Ling, H. Zandbergen, C. Dekker, *Nat. Mater.* **2003**, *2*, 537–540; e) J. Li, D. Stein, C. McMullan, D. Branton, M. J. Aziz, J. A. Golovchenko, *Nature* **2001**, *412*, 166–169; f) H. Craighead, *Nature* **2006**, *442*, 387–393; g) N. Li, S. Yu, C. C. Harrell, C. R. Martin, *Anal. Chem.* **2004**, *76*, 2025–2030; h) A. L. Sisson, M. R. Shah, S. Bhosale, S. Matile, *Chem. Soc. Rev.* **2006**, *35*, 1269–1286.

[14] a) S. O. Kim, H. H. Solak, M. P. Stoykovich, N. J. Ferrier, J. J. de Pablo, P. F. Nealey, *Nature* **2003**, *424*, 411–414; b) M. Park, C. Harrison, P. M. Chaikin, R. A. Register, D. H. Adamson, *Science* **1997**, *276*, 1401–1404; c) F. S. Bates, G. H. Fredrickson, *Phys. Today* **2008**, *52*, 32–38; d) C. Park, J. Yoon, E. L. Thomas, *Polymer* **2003**, *44*, 6725–6760; e) K.-V. Peinemann, V. Abetz, P. F. Simon, *Nat. Mater.* **2007**, *6*, 992–996; f) S. I. Stupp, V. LeBonheur, K. Walker, L.-S. Li, K. E. Huggins, M. Keser, A. Amstutz, *Science* **1997**, *276*, 384–389; g) H. Gleiter, *Appl. Phys. Lett.* **2000**, *48*, 1–29.

[15] a) H.-Y. Hsueh, C.-T. Yao, R.-M. Ho, *Chem. Soc. Rev.* **2015**, *44*, 1974–2018; b) M. A. Hillmyer, *Adv. Polym. Sci.* **2005**, *190*, 137–181; c) J. Bang, S. H. Kim, E. Drockenmuller, M. J. Misner, T. P. Russell, C. J. Hawker, *J. Am. Chem. Soc.* **2006**, *128*, 7622–7629; d) M. Kang, B. Moon, *Macromolecules* **2009**, *42*, 455–458; e) H. Zhao, W. Gu, M. W. Thielke, E. Sterner, T. Tsai, T. P. Russell, E. B. Coughlin, P. Theato, *Macromolecules* **2013**, *46*, 5195–5201; f) X. Sui, Z. Zhang, S. Guan, Y. Xu, C. Li, Y. Lv, A. Chen, L. Yang, L. Gao, *Polym. Chem.* **2015**, *6*, 2777–2782; g) M.-S. She, T.-Y. Lo, H.-Y. Hsueh, R.-M. Ho, *NPG Asia Mater.* **2013**, *5*, e42; h) M. Zhang, L. Yang, S. Yurt, M. J. Misner, J.-T. Chen, E. B. Coughlin, D. Venkataraman, T. P. Russell, *Adv. Mater.* **2007**, *19*, 1571–1576.

[16] a) H. Zhao, E. S. Sterner, E. B. Coughlin, P. Theato, *Macromolecules* **2012**, *45*, 1723–1736; b) J.-F. Gohy, Y. Zhao, *Chem. Soc. Rev.* **2013**, *42*, 7117–7129; c) H. Zhao, W. Gu, R. Kakuchi, Z. Sun, E. Sterner, T. P. Russell, E. B. Coughlin, P. Theato, *ACS Macro Lett.* **2013**, *2*, 966–969.

[17] a) J. W. Diggle, T. C. Downie, C. Goulding, *Chem. Rev.* **1969**, *69*, 365–405; b) W. Lee, S.-J. Park, *Chem. Rev.* **2014**, *114*, 7487–7556; c) H. Masuda, H. Yamada, M. Satoh, H. Asoh, M. Nakao, T. Tamamura, *Appl. Phys. Lett.* **1997**, *71*, 2770–2772.

[18] a) Y. Honmou, S. Hirata, H. Komiyama, J. Hiyoshi, S. Kawauchi, T. Iyoda, M. Vacha, *Nat. Commun.* **2014**, *5*, 4666; b) A. Rehab, N. Salahuddin, *Polymer* **1999**, *40*, 2197–2207; c) F. B. Kaufman, E. M. Engler, *J. Am. Chem. Soc.* **1979**, *101*, 547–549.

[19] Y.-D. Zhang, R. D. Hreha, G. E. Jabbour, B. Kippelen, N. Peyghambarian, S. R. Marder, *J. Mater. Chem.* **2002**, *12*, 1703–1708.

[20] T. Stephan, S. Muth, M. Schmidt, *Macromolecules* **2002**, *35*, 9857–9860.

[21] H. Tunell, M. Selo, K. Skarp, J. Hilborn, *Polym. J.* **2006**, *38*, 716–723.

[22] Y. Shim, H.-J. Lee, S. Lee, S.-H. Moon, J. Cho, *Environ. Sci. Technol.* **2002**, *36*, 3864–3871.

[23] S. Chang, S. Singamaneni, E. Kharlampieva, S. L. Young, V. V. Tsukruk, *Macromolecules* **2009**, *42*, 5781–5785.

Received: July 4, 2016
Revised: August 22, 2016
Published online: September 21, 2016

